PAPER

High-quality CsPbBr₃ perovskite nanocrystals for quantum dot light-emitting diodes†

Xiafang Du,‡[a] Guan Wu,‡[a] Jian Cheng,[a] Hui Dang,[a] Kangzhe Ma,[a] Ya-Wen Zhang,[a] Peng-Feng Tan[a] and Su Chen*[ab]

Metal halide perovskites, such as CsPbX₃ (X = Cl, Br, and I), have gained extensive attention due to their increasing demand in optoelectronic applications such as solar cells and lighting-emitting devices. Herein, we report a versatile approach to synthesize high-quality CsPbBr₃ perovskite nanocrystals (sized 5–15 nm) by ligand-assisted reprecipitation at room temperature. The monodispersed CsPbBr₃ nanocube perovskites displayed relatively high photoluminescence quantum yields of 50–80%. By virtue of the quantum size effects, the bandgap energies were manipulated from blue to green spectral regions (410–530 nm). In addition, through compositional modulations of the anion exchange technique, the bright photoluminescence could be almost tuned over the entire visible spectral region (450–650 nm). Furthermore, the photoluminescence of the CsPbBr₃ nanocrystals was characterized by narrow emission line widths of 15–50 nm and radiative lifetimes of 5–15 ns. Finally, by taking advantage of these outstanding merits, the CsPbBr₃ perovskites were successfully utilized in the application of highly fluorescent patterning and color-purity light-emitting diodes.

Introduction

Halide perovskites have attracted significant interests in a variety of optoelectronic applications, including solar cells,[1,2] light-emitting diodes (LEDs),[3,4] photodetectors,[5,6] and lasers,[7,8] due to their high photoluminescence,[9] excellent stability,[10] and low-threshold lasing.[11] Halide perovskites mainly contain two categories: organic–inorganic hybrid perovskites (APbX₃, where A stands for the small molecular organic amine, such as CH₃NH₃⁺, and X represents a halide, such as Br, I, and Cl) and all-inorganic halide perovskites (CsPbX₃). For the organic–inorganic hybrid perovskites,[12–14] the facile and low-cost preparation process can be utilized to yield high-quality perovskite nanocrystals (NCs). Wong *et al.* reported a versatile strategy to prepare color-tunable CH₃NH₃PbBX₃ perovskite nanorod arrays through an anion exchange technique at low temperature.[15] Zhang *et al.* fabricated brightly luminescent colloidal CH₃NH₃PbX₃ NCs with an absolute photoluminescence (PL) quantum yield (QY) of upto 70% at room temperature *via* a ligand-assisted reprecipitation (LARP) strategy.[16] However, the relatively low PLQYs of organic–inorganic hybrid perovskites severely discourage their further development and potential application.

Recently, all-inorganic halide perovskites (such as CsPbX₃, X = Cl, Br, and I), which can present relatively higher PLQYs compared with organic–inorganic hybrid perovskites,[17,18] are emerging in perovskites family. In this respect, Protesescu *et al.* reported a facile colloidal synthesis of monodispersed CsPbX₃ nanocubes at high temperature, which displayed a high PLQY of upto 90%, as well as a bright emission with a wide color gamut. The PL emission spectra of CsPbX₃ perovskites could be tuned over the entire visible spectral region (410–700 nm).[19] In addition, Song *et al.* synthesized high-quality CsPbX₃ quantum dots (QDs) through a hot injection method and first developed the quantum dots-based QLEDs with sharp emissions.[20] To further achieve the high-quality CsPbX₃ perovskites at low temperature, Li *et al.* developed a supersaturated recrystallization method for the synthesis of CsPbX₃ perovskites in the application of white LEDs. Excellent PL with high QY upto 95%, white LEDs with tunable color temperature, and a wide color gamut were obtained.[21] It is because of the high PLQY that CsPbX₃ perovskites are widely used in optoelectronic applications.

Herein, we report a high-quality colloidal CsPbBr₃ perovskites NCs (sized 5–15 nm) synthesized at room temperature using a new precursor: cesium bromide (CsBr). The monodispersed CsPbBr₃ nanocube perovskites exhibited relatively high PLQY (50–80%) and size-tunability of their bandgap energies that were manipulated from the blue to green spectral regions (410–530 nm). The PL of CsPbBr₃ NCs also possessed

[a]State Key Laboratory of Materials-Oriented Chemical Engineering, College of Chemistry and Chemical Engineering, Nanjing Tech University (former: Nanjing University of Technology), Nanjing 210009, P. R. China. E-mail: chensu@njtech.edu.cn; Fax: +86-25-83172258; Tel: +86-25-83172258

[b]Jiangsu Key Lab of Fine Chemical & Functional Polymer Materials, P. R. China

† Electronic supplementary information (ESI) available. See DOI: 10.1039/c6ra27665b

‡ Contributed equally to this work.

narrow emission line widths of 15–50 nm and radiative lifetimes of 5–15 ns. In addition, *via* utilizing the anion exchange reaction technique, the bright PL could nearly be tuned over the entire visible spectral region (450–650 nm). Moreover, when considering cation exchange (MA^+ and Cs^+), the hybrid perovskites exhibited a high QY and narrow emission. Finally, we successfully designed highly luminescent patterning and color-purity LEDs using $CsPbBr_3$ perovskite NCs, where the LED maintained the low turn-on voltages and narrow full-width at half maxima (FWHM) emission.

Experimental

Materials

Lead(II) bromide ($PbBr_2$, 99%), methylamine (CH_3NH_2, 33 wt% in absolute ethanol), *n*-octylamine (99%), dodecylamine (98%), oleylamine (90%), hydrochloric acid (HCl, 37 wt%), hydrobromic acid (HBr, 48 wt%), hydriodic acid (HI, 57 wt%), and oleic acid (90%) were purchased from Aladdin Chemistry Co., Ltd. *N,N*-Dimethylformamide (DMF), cesium bromide (CsBr), toluene, cyclohexane, dichloromethane, and chloroform were purchased from Sinopharm Chemical Reagent Co., Ltd (Shanghai, China). All reagents were used without further purification.

Fabrication of the colloidal perovskite $CsPbBr_3$ NCs

Colloidal perovskite $CsPbBr_3$ NCs were fabricated by the LARP technique, which has been described as follows. In a typical synthesis, a mixture of 0.1 mmol CsBr and 0.2 mmol $PbBr_2$ was dissolved in 5 mL of DMF *via* ultrasonication, and then 20 μL of *n*-octylamine and 0.5 mL of oleic acid were added to form a precursor solution. A 250 μL of precursor solution was added to 10 mL of toluene under vigorous stirring. A bright green solution could be immediately observed. After centrifugation at 12 000 rpm for 10 min to discard the precipitates, a bright blue-green colloidal solution was obtained. Other $CsPbBr_3$ NCs were fabricated using different solvents, precursors, and ligands based on a similar LARP strategy.

Synthesis of CH_3NH_3X (MAX, X = Cl and I)

CH_3NH_3X (X = Cl and I) was prepared using an approach described in the literature.[22] First, methylamine was dissolved in absolute ethanol under stirring at 0 °C for 2 h. Then, the corresponding acid was added to the abovementioned solution and it was left to react for 2 h at 0 °C under continuous stirring. After this, the solvent was removed by rotary evaporation with a pressure of 0.1 MPa at 50 °C. After rotary evaporation, the precipitate powders were collected and washed three times (diethylether) and dried in a vacuum oven (60 °C, 5 h).

Ion-exchange reactions

Ion-exchange with solid methylamine halide salts (MAX, X = Cl and I) were performed by adding different quantities (normally ranging from 1 to 2 mmol) of MAX solid salt to a rapidly stirred crude colloidal perovskite $CsPbBr_3$ NCs solution (10 mL toluene).

Device fabrication

Solutions of ZnO nanocrystals were spin-coated on the ITO-coated glass substrates at 4000 rpm for 50 s and annealed in air at 200 °C. Perovskite solutions were spin-coated on the ZnO films to prepare a perovskite film (in the range of 125–150 nm). Then, a 25 nm thin layer of TFB was spin-coated using a *m*-xylene solution (10 mg mL^{-1}) at 2500 rpm. Finally, the MoO_x/Au electrodes were deposited using a thermal evaporation system.

Characterization

Ultraviolet-visible (UV-vis) absorption spectra were obtained using a Perkin-Elmer Lambda 950 spectrometer. Photoluminescence (PL) measurements were carried out using a Varian Cary Eclipse spectrophotometer. The photoluminescence quantum yield (PLQY) was estimated according to a standard procedure using appropriate dye molecules for the blue, green, and red spectral regions (coumarin 343, fluorescein, and rhodamine 6G). X-ray diffraction (XRD) was performed *via* a Rigaku Corporation D/max-rC rotating anode X-ray powder diffractometer using a copper target. Transmission electron microscopy (TEM) images were obtained using a Tecnai G2 F30 S-TWIN transmission electron microscope. X-ray photoelectron (XPS) spectra were acquired using an ES-CAIAB250 XPS system with an Al/Kα source, and the energy step size was set at 0.100 eV. Energy dispersive X-ray (EDX) analysis was performed using two scanning electron microscopes (Zeiss Gemini 1530 and Hitachi, S-4800). TCSPC data were performed using an Edinburgh FL 900 photo counting system. LED devices were measured using a Keithley 2400 source meter and a fiber integration sphere (FOIS-1) coupled with a QE-6500 spectrometer was used for room temperature measurements under ambient conditions.

Results and discussion

The colloidal $CsPbBr_3$ NCs were synthesized *via* a simple and versatile LARP technique and a schematic of the detailed operation is shown in Fig. 1. A mixture of CsBr, $PbBr_2$, oleic acid, and the assisted-ligand of *n*-octylamine was dissolved in *N*-dimethylformamide (DMF), ultrasonicated, and a uniform free-standing layered precursor solution was formed (Fig. 1a).[23] Then, the precursor solution was gradually added into a vigorously stirred non-polar solvent (toluene, dichloromethane, *etc.*). After this, a blue-green colloidal solution was formed, implying an aggregation process of the precursor into nanoparticles.[22] It was also revealed that the crystallization process was controlled by supersaturation, which was initially induced by the solubility change with solvent mixing.[18] Finally, a high-quality colloidal solution was achieved, which is clearly seen from the optical image shown in Fig. 1b. *Via* utilizing the high PL properties of $CsPbX_3$ perovskites, a "taiji" patterning (Fig. 1c) and LEDs (Fig. 1d) with saturated color-purity were obtained.

The morphology, phase structure, and composition features are shown in Fig. 2. TEM image of the $CsPbBr_3$ NCs is illustrated in Fig. 2a, which displays the cube shape and an average diameter of 7.45 nm with a size deviation of ±0.5 nm (Fig. 2b).
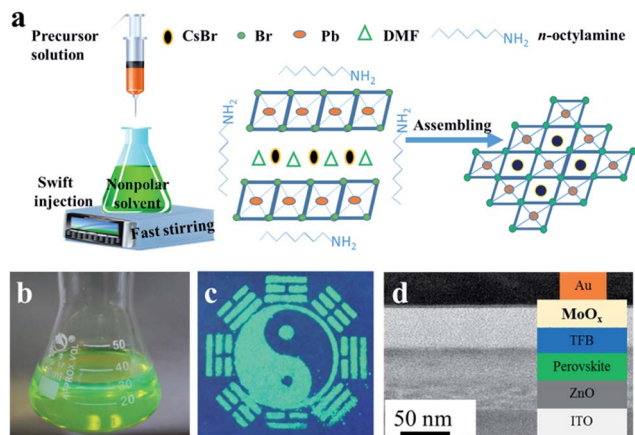
Fig. 1 (a) Schematic of the prepared process for colloidal $CsPbBr_3$ perovskite NCs, and the precursor solution and assembly into NCs. (b) The optical image of the colloidal nanocrystal solution. (c) The highly luminescent $CsPbBr_3$ NCs-PMMA polymer patterning, and (d) LEDs using $CsPbBr_3$ NCs.
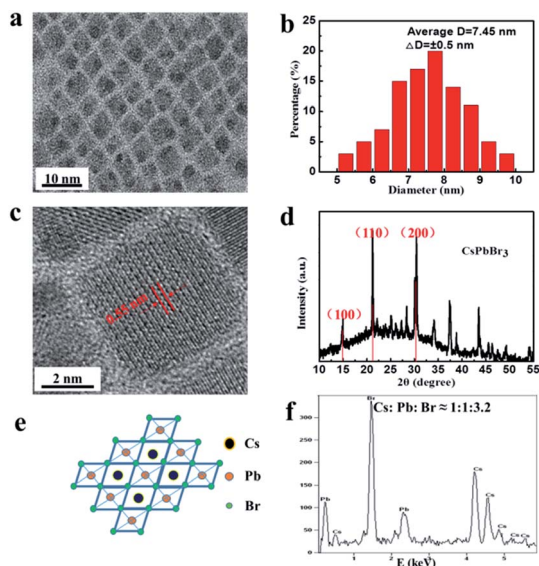

Fig. 2 (a) TEM image of the colloidal $CsPbBr_3$ NCs. (b) Size distribution analysis for the sample. (c) High-resolution TEM image of the colloidal $CsPbBr_3$ NCs. (d) XRD patterns of the colloidal $CsPbBr_3$ NCs. (e) Molecular structure model, and (f) EDX spectrum of the colloidal $CsPbBr_3$ NCs.

The phase structure of the as-synthesized samples was further characterized by HRTEM and XRD patterns. It was observed that the lattice fringes of the NCs were 0.55 nm (Fig. 2c), corresponding to the (100) crystal faces.[19] From the XRD patterns (Fig. 2d), the (100), (110), and (200) peaks demonstrated the cubic crystal structure of $CsPbBr_3$ NCs.[9,24] Fig. 2e shows the molecular structural model of $CsPbBr_3$ NCs, which clarified that the ideal Cs : Pb : Br atomic ratio was close to 1 : 1 : 3 for the perovskite NCs. The detailed EDX result, as shown in Fig. 2f, reveals that the atomic ratio of the NCs was 1 : 1 : 3.2 (see Table S1†), which was close to the theoretical value. The elemental

analysis was carried out *via* XPS (Fig. S1a†). As described in Fig. S1b–d,† the XPS showed the Cs 3d peaks at 726 eV and 740 eV, Pb 4f peaks at 141 eV and 146 eV, and the fitted two peaks of Br 3d at 69 eV and 71 eV.

The optical properties of the colloidal $CsPbBr_3$ perovskite NCs were further investigated utilizing UV-vis absorption and PL spectroscopies. As described in Fig. 3a, the colloidal $CsPbBr_3$ NCs present the absorption (red) and emission (black) spectra. A band edge at about 500 nm could be clearly observed in the UV-vis absorption spectrum. The $CsPbBr_3$ NCs displayed a sharp emission peak position centered at 518 nm with a narrow FWHM value of only 18 nm from the PL spectrum, suggesting superior color saturation of the NCs (see the inset of Fig. 3a). The PLQY of the colloidal $CsPbBr_3$ NCs was estimated to be 50–80%, which could be compared to the coated chalcogenide NCs.[25,26] We further investigated the time-resolved PL decay of the $CsPbBr_3$ NCs (Fig. 3b). The PL decay curve was fitted to the biexponential decay functions, and the radiative lifetimes were in the range of 5–20 ns.

The LARP method is a versatile technique to fabricate NCs *via* a solvent mixing approach and it is also a useful strategy to manipulate the size and morphology of the NCs *via* introducing capped ligands on the nanoparticles surface. It was reported that long-chain ligands could control the NCs size and the solvent polarity had a role in restraining the aggregation effects. Hence, we comprehensively investigated the solvent polarity, long-chain ligands (alkylamine with long chains), and the amount of ligands and precursor to affect the fluorescence properties (Fig. S2†). As illustrated in Fig. S2a,† PL showed a red shift effect with the increasing solvent polarity. Additionally, the red shift effect was obviously seen by increasing the alkyl chains of the capping ligand, as shown in Fig. S2b.† Furthermore, with the increasing amount of precursor, the red shift effect of PL was seriously decreased (Fig. S2c†). However, the blue shift effect of the PL intensity was increased after increasing the amount of ligand (Fig. S2d†). Thus, the added solvent polarity, ligand, and the amount of ligands and precursor could significantly influence the PL properties.

To further tune the wide spectra of the NCs PL, we adopted ion-exchange to realize the color of NCs by mixing the as-prepared $CsPbBr_3$ NCs and MAX (X = Cl and I). We simultaneously investigated the effects of anion-exchange (halide source) and cation-exchange (MA^+ and Cs^+). The size and shape characteristics of the $CsPbX_3$ NCs by ion-exchange manipulation can be clearly seen in Fig. 4. It is superior to those directly
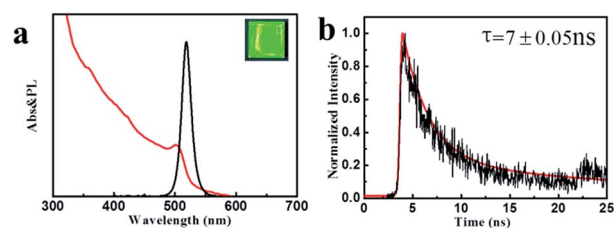

Fig. 3 (a) UV-vis absorption and PL emission spectra (inset: image (λ_{ex} = 365 nm) $CsPbX_3$ NCs). (b) Time-resolved PL decay and fitting curve for the colloidal $CsPbBr_3$ NCs sample.
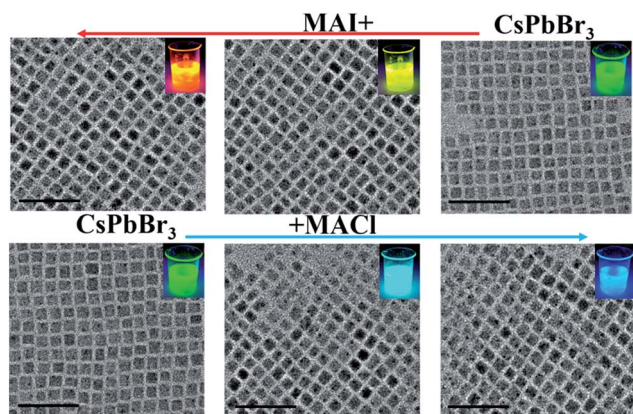
Fig. 4 TEM images of the CsPbBr$_3$ NCs after treatment with various quantities of MAI (up) and MACl (down). The insets show the evolution of emission colors (under a UV lamp, λ_{ex} = 365 nm) from crude CsPbBr$_3$ NCs to composited perovskite NCs. Scale bars correspond to 50 nm.
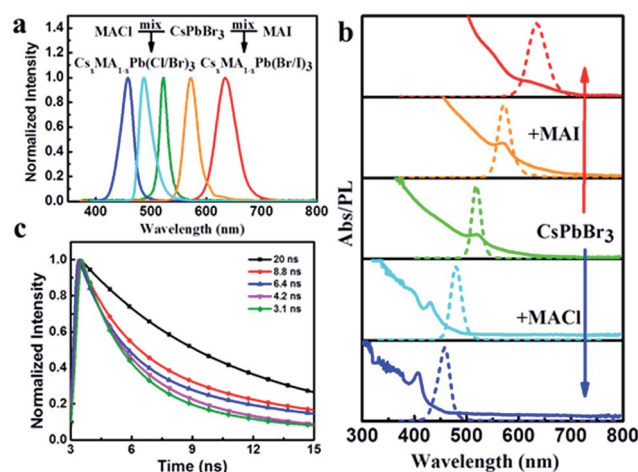

Fig. 5 (a) An overview of the PL spectra of the samples obtained by mixing CsPbBr$_3$ NCs with either MACl or MAI NCs in various ratios (λ_{ex} = 365 nm for all). (b) Evolution of the optical absorption (solid lines) and PL (dashed lines) spectra of CsPbBr$_3$ NCs with the increasing quantities of MAX (X = Cl and I), added as ion-exchange sources. (c) Evolution of the time-resolved PL decay spectra of CsPbBr$_3$ NCs and mixing with either MACl or MAI NCs at various ratios.

synthesized with mixed-halides CsPbX$_3$ at low temperature, which obtained either bulk or poorly polydispersed non-luminescent crystallites. It was also suggested that our ion-exchanged samples could even be comparable to the directly synthesized mixed-halides CsPbX$_3$ sample at high temperature. The molar ratios between MA$^+$ ions and Cs$^+$ ions were further determined by EDX measurements (Table S2†). Therefore, we considered that the reaction between MAX and CsPbBr$_3$ in a non-stoichiometric ratio resulted in the formation of (Cs)$_x$(MA)$_{1-x}$Pb(Cl/Br)$_3$ or (Cs)$_x$(MA)$_{1-x}$Pb(Br/I)$_3$ intermediate complex.

The bright PL of perovskite NCs (Fig. S3a†) could be tuned over almost the entire visible spectral region (450–650 nm). As observed from the PL spectra, as shown in Fig. 5a and b, the resulting composition of the ion-exchanged NCs were Stokes-shifted with respect to the optical absorption spectra and the NCs possessed a narrow FWHM of 10–40 nm, as previously reported.[19] The PLQY of the samples generally dropped from the starting value of 82% after mixing the as-prepared CsPbBr$_3$ NCs with either MACl or MAI (Fig. S3b†). Time-resolved photo-luminescence decays of the resulting composition indicated the radiative lifetimes in the range of 1–20 ns. In general, the life-times of the resulting composition were increased with an increase of I-ions and decreased with an increase of Cl-ions (Fig. 5c).

It is well-known that the high speed of anion-exchange in the perovskite NCs is rooted in the ionic conductivity of halides.[27] However, after using MAX (X = Cl and I), the cation (MA$^+$) could be also engaged in ion-exchange reactions and raised a further complication, resulting in the replacement of Cs$^+$ (1.81 Å) ions with the larger MA$^+$ (2.70 Å) ions. According to the Fourier transform infrared spectroscopy (FTIR) analysis, we could obviously see the peaks intensity significantly strengthened at 2800 and 2900 cm^{-1}, corresponding to stretching vibration of N–H (Fig. S4†).[28] It was revealed that Cs$^+$ ions replaced MA$^+$ ions. To further demonstrate the ion-replacement, XRD was performed (Fig. S5†). From the lattice parameters change of the

XRD patterns, we could infer the replacement of Cs$^+$ ions with MA$^+$ ions. However, the ion-exchange reactions almost had no influence on the shape and cubic structure of the starting CsPbBr$_3$ sample under low temperature of the ion-exchange reaction.

Light-emission applications[29] generally demand compatibility of the NC-emitters with matrix materials. To demonstrate this miscibility, the CsPbBr$_3$ NCs were embedded into poly-(methylmethacrylate) (PMMA) forming well dispersed composites where the composites yielded excellent optical clarity and bright emission. Concomitantly, the versatile fluorescent patterns were further achieved by silk screen printing, which is a widely used and effective technique.[30] As shown in Fig. 6a, a mixture of PMMA and CsPbBr$_3$ NCs acting as printing ink was cast onto a mask (160 meshes screen), and the ink was infiltrated through the patterned mask onto the substrate by scraping the ink. Fig. 6b–d show the designed patterns of "NJTU" and "taiji". The pattern was invisible under daylight (Fig. 6c), whereas it was remarkably visible under UV light (Fig. 6d). It was revealed that the patterns possessed both "vis-
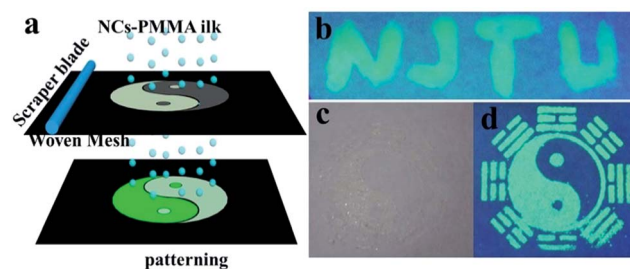

Fig. 6 (a) The schematic of patterning by screen printing. (b), (d) Images (λ_{ex} = 365 nm) and (c) (under daylight) of the patterning obtained using the mixture of CsPbBr$_3$ NC-PMMA.
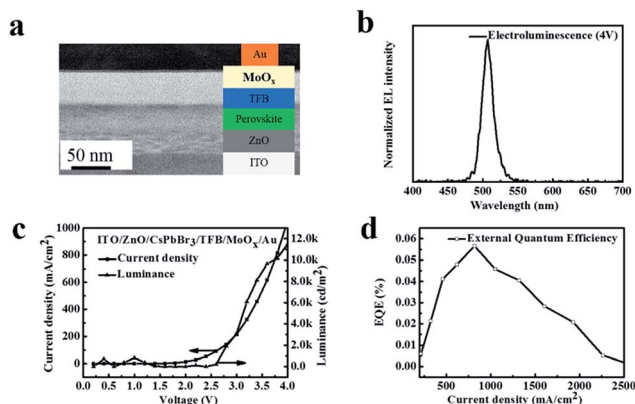
Fig. 7 (a) Device structure of the CsPbBr₃ perovskite LEDs. Schematic and the cross-sectional TEM image of the device: ITO/ZnO/perovskite/TFB/MoO$_x$/Au. (b) Normalized EL spectrum of the CsPbBr₃ perovskite thin film-based LEDs at the applied voltage of 4 V. (c) Current density and luminance for the CsPbBr₃ perovskite LED measured at room temperature. (d) The external quantum efficiency (EQE) *versus* current density curves of this LED.

invisible" and "UV-visible" properties, which has potential application in the anti-counterfeit and labelling fields.

To design the practical application of the as-synthesized CsPbBr₃ perovskite in optoelectronic devices, bright green electroluminescence (EL) LEDs were fabricated. The LED device consisted of multiple layers of ITO/ZnO/CsPbBr₃/TFB/MoO$_x$/Au (Fig. 7a): indium tin oxide (ITO) was coated on the glass substrate, 40 nm ZnO NCs were employed as electron-transporting and hole-blocking layers, the 25 nm poly(9,9-dioctyl-fluorene-*co*-*N*-(4-butylphenyl)diphenylamine) (TFB) served as the hole-transporting and electron-blocking inter-layers, 10 nm molybdenum trioxide, and 100 nm gold (Au) electrode acted as a hole selective contact. Fig. 7b shows the EL spectra of the device under a bias of 4 V. The EL emission peak at 510 nm with a narrow FWHM of 20 nm and the shape of the EL spectrum did not change, indicating that the carriers were well confined within the perovskite layers. Fig. 7c presents the current density and luminescence *versus* driving voltage. The device displayed a turn on voltage of 3 V at room temperature. The current density and luminance rapidly increased after turning on the voltage, suggesting a very low series resistance and efficient operation of the LED device. The CsPbBr₃ perovskite LEDs device presented a peak external quantum efficiency (EQE) at around 0.06% at ~4 V (Fig. 7d), which is comparable to the previously reported studies.[4,31]

Conclusions

In summary, we synthesized highly luminescent colloidal CsPbBr₃ NCs with high QY (QY = 50–80%) and highly bright blue and green emission (410–530 nm) using a simple and versatile LARP technique. Additionally, the post synthetic chemical transformations (ion-exchange, (MAX, X = Cl, I)) approach was utilized to achieve a wide variety of complex perovskite NCs, which displayed a visible spectral region of the

PL spectrum (450–650 nm), and the PL is also affected by both the cation and anion exchange processes. Furthermore, we have constructed high color-purity LED using CsPbBr₃ perovskite nanocrystals, which maintains the low turn-on voltages and narrow full-width at half maxima (FWHM) emission. We believe our results will guide the development of perovskites and open an avenue towards the design of high-performance optoelectronic devices.

Acknowledgements

Notes and references

1 N. J. Jeon, J. H. Noh, Y. C. Kim, W. S. Yang, S. Ryu and S. I. Seok, *Nat. Mater.*, 2014, **13**, 897–903.

2 D. Li, P. Liao, X. Shai, W. Huang, S. Liu, H. Li, Y. Shen and M. Wang, *RSC Adv.*, 2016, **6**, 89356–89366.

3 Z. K. Tan, R. S. Moghaddam, M. L. Lai, P. Docampo, R. Higler, F. Deschler, M. Price, A. Sadhanala, L. M. Pazos, D. Credgington, F. Hanusch, T. Bein, H. J. Snaith and R. H. Friend, *Nat. Nanotechnol.*, 2014, **9**, 687–692.

4 Y. Ling, Z. Yuan, Y. Tian, X. Wang, J. C. Wang, Y. Xin, K. Hanson, B. Ma and H. Gao, *Adv. Mater.*, 2016, **28**, 305–311.

5 L. Dou, Y. M. Yang, J. You, Z. Hong, W. H. Chang, G. Li and Y. Yang, *Nat. Commun.*, 2014, **5**, 5404.

6 L. Su, Z. X. Zhao, H. Y. Li, J. Yuan, Z. L. Wang, G. Z. Cao and G. Zhu, *ACS Nano*, 2015, **9**, 11310–11316.

7 G. Xing, N. Mathews, S. S. Lim, N. Yantara, X. Liu, D. Sabba, M. Gratzel, S. Mhaisalkar and T. C. Sum, *Nat. Mater.*, 2014, **13**, 476–480.

8 Y. Fu, H. Zhu, C. C. Stoumpos, Q. Ding, J. Wang, M. G. Kanatzidis, X. Zhu and S. Jin, *ACS Nano*, 2016, **10**, 7963–7972.

9 A. Swarnkar, R. Chulliyil, V. K. Ravi, M. Irfanullah, A. Chowdhury and A. Nag, *Angew. Chem., Int. Ed.*, 2015, **54**, 15424–15428.

10 S. Huang, Z. Li, L. Kong, N. Zhu, A. Shan and L. Li, *J. Am. Chem. Soc.*, 2016, **138**, 5749–5752.

11 Y. Wang, X. Li, X. Zhao, L. Xiao, H. Zeng and H. Sun, *Nano Lett.*, 2016, **16**, 448–453.

12 Y. S. Zhao, H. Fu, A. Peng, Y. Ma, D. Xiao and J. Yao, *Adv. Mater.*, 2008, **20**, 2859–2876.

13 F. Zhu, L. Men, Y. Guo, Q. Zhu, U. Bhattacharjee, P. M. Goodwin, J. W. Petrich, E. A. Smith and J. Vela, *ACS Nano*, 2015, **9**, 2948–2959.

14 C. Lee, J. Hong, A. Stroppa, M.-H. Whangbo and J. H. Shim, *RSC Adv.*, 2015, **5**, 78701–78707.

15 A. B. Wong, M. Lai, S. W. Eaton, Y. Yu, E. Lin, L. Dou, A. Fu and P. Yang, *Nano Lett.*, 2015, **15**, 5519–5524.

16 F. Zhang, H. Zhong, C. Chen, X.-g. Wu, X. Hu, H. Huang, J. Han, B. Zou and Y. Dong, *ACS Nano*, 2015, **9**, 4533–4542.

17 J. Li, X. Yuan, P. Jing, J. Li, M. Wei, J. Hua, J. Zhao and L. Tian, *RSC Adv.*, 2016, **6**, 78311–78316.

18 G. Nedelcu, L. Protesescu, S. Yakunin, M. I. Bodnarchuk, M. J. Grotevent and M. V. Kovalenko, *Nano Lett.*, 2015, **15**, 5635–5640.

19 L. Protesescu, S. Yakunin, M. I. Bodnarchuk, F. Krieg, R. Caputo, C. H. Hendon, R. X. Yang, A. Walsh and M. V. Kovalenko, *Nano Lett.*, 2015, **15**, 3692–3696.

20 J. Song, J. Li, X. Li, L. Xu, Y. Dong and H. Zeng, *Adv. Mater.*, 2015, **27**, 7162–7167.

21 X. Li, Y. Wu, S. Zhang, B. Cai, Y. Gu, J. Song and H. Zeng, *Adv. Funct. Mater.*, 2016, **26**, 2435–2445.

22 S. Sun, D. Yuan, Y. Xu, A. Wang and Z. Deng, *ACS Nano*, 2016, **10**, 3648–3657.

23 Y. Niu, F. Zhang, Z. Bai, Y. Dong, J. Yang, R. Liu, B. Zou, J. Li and H. Zhong, *Adv. Opt. Mater.*, 2015, **3**, 112–119.

24 C. C. Stoumpos, C. D. Malliakas, J. A. Peters, Z. Liu, M. Sebastian, J. Im, T. C. Chasapis, A. C. Wibowo, D. Y. Chung, A. J. Freeman, B. W. Wessels and M. G. Kanatzidis, *Cryst. Growth Des.*, 2013, **13**, 2722–2727.

25 P. Maity, T. Debnath and H. N. Ghosh, *J. Phys. Chem. C*, 2015, **119**, 26202–26211.

26 K. W. Song, R. Costi and V. Bulović, *Adv. Mater.*, 2013, **25**, 1420–1423.

27 J. Mizusaki, K. Arai and K. Fueki, *Solid State Ionics*, 1983, **11**, 203–211.

28 S. Zhu, Q. Meng, L. Wang, J. Zhang, Y. Song, H. Jin, K. Zhang, H. Sun, H. Wang and B. Yang, *Angew. Chem., Int. Ed. Engl.*, 2013, **52**, 3953–3957.

29 F. Meinardi, A. Colombo, K. A. Velizhanin, R. Simonutti, M. Lorenzon, L. Beverina, R. Viswanatha, V. I. Klimov and S. Brovelli, *Nat. Photonics*, 2014, **8**, 392–399.

30 S.-S. Liu, C.-F. Wang, C.-X. Li, J. Wang, L.-H. Mao and S. Chen, *J. Phys. Chem. C*, 2014, **2**, 6477.

31 N. Yantara, S. Bhaumik, F. Yan, D. Sabba, H. A. Dewi, N. Mathews, P. P. Boix, H. V. Demir and S. Mhaisalkar, *J. Phys. Chem. Lett.*, 2015, **6**, 4360–4364.